Formation of substances with humic-like fluorescence properties, upon photoinduced oligomerization of typical phenolic compounds emitted by biomass burning

Formation of substances with humic-like fluorescence properties, upon photoinduced oligomerization of typical phenolic compounds emitted by biomass burning

Davide Vione,[a,*] Alexandre Albinet,[b] Francesco Barsotti,[a†] Majda Mekic,[c,d] Bin Jiang,[c] Claudio Minero,[a] Marcello Brigante,[e] Sasho Gligorovski[c]

[a] *Dipartimento di Chimica, Università di Torino, Via Pietro Giuria 5, 10125 Torino, Italy.*

[b] *INERIS, Parc Technologique Alata BP2, 60550 Verneuil en Halatte, France.*

[c] *State Key Laboratory of Organic Geochemistry, Guangzhou Institute of Geochemistry, Chinese Academy of Sciences, Guangzhou 510 640, China.*

[d] *University of Chinese Academy of Sciences, Beijing 10069, China*

[e] *Université Clermont Auvergne, CNRS, SIGMA Clermont, Institut de Chimie de Clermont-Ferrand, F-63000 Clermont-Ferrand, France.*

† *Current address: SMAT SpA, Corso XI Febbraio 14, 10152 Torino, Italy.*

* Corresponding author. E-mail: *davide.vione@unito.it*. Tel. +39-011-6705296.

Abstract

The irradiation under simulated sunlight of some phenolic compounds typically emitted in ambient air by biomass burning, namely vanillin and acetosyringone, yielded intermediates with humic-like fluorescence properties that can be assimilated to humic-like substances (HULIS). Evidence was obtained by ultra-high-resolution mass spectrometry of the occurrence of oligomerization processes up to the formation of trimeric species. In contrast,

the irradiation of other biomass-burning compounds such as vanillic acid, m-cresol and guaiacol did not yield either HULIS-type fluorescence or oligomers. We suggest that the photolysis of biomass-burning compounds is a potential HULIS source in the atmosphere, if the relevant substrates undergo photoinduced oligomerization reactions.

Keywords: Aerosol; Biomass burning, HuLiS, Photolysis; Methoxyphenols.

Introduction

Atmospheric aerosols play important roles in several aspects of atmospheric chemistry and physics, including most notably their effects on albedo and climate (with positive or negative feedback depending on the aerosol chemical composition; Schwartz and Andreae, 1996; Boucher et al., 2013), on precipitation (cloud condensation nuclei activity; Rosenfeld et al., 2008) and on air pollution including human health (Dockery et al., 1992; Heal et al., 2012). An interesting aspect of airborne aerosols is the possibility to be covered by a water film that in some cases may grow up to form cloud/fog droplets. However, even a thin water film provides a liquid phase (sometimes a very concentrated one) for important atmospheric processes to occur. These processes may be involved in the generation of compounds that further act as precursors of secondary organic aerosols (SOA), thereby potentially increasing the aerosol loading in the atmosphere (McNeill et al., 2012).

The occurrence of a water layer on the surface of particles depends on the level of moisture, but it is also linked to the presence of hygroscopic compounds such as inorganic salts and the so-called humic-like substances (HULIS) (Chan and Chan, 2003; Ruehl et al., 2016). HULIS

may originate from both, primary (biomass burning and the associated dust) and secondary emission sources (SOA) (Srivastava et al., 2018). They are operationally defined based on optical/luminescent properties that closely resemble those of humic substances found in natural waters. These properties include peculiar fluorescence behavior and an absorption spectrum that undergoes a featureless decay with wavelength up to the visible region (Graber and Rudich, 2006; Krivácsy et al., 2008). While HULIS are possibly not so humic-like as initially thought (they have lower molecular weight and are more oxygen-rich than humic substances; Graber and Rudich, 2006), the undeniable similarities justify research into the nature of the chromophores and fluorophores of both HULIS and humic compounds.

Several previous papers have reported that colored species with HULIS fluorescence properties are formed by photoinduced oxidation of compounds such as phenol and its dimer 4-phenoxyphenol (Chang and Thompson, 2010; De Laurentiis et al., 2013a/b). Moreover, some phenols that can absorb the UV fraction of the sunlight radiation (e.g., tyrosine as well as 4-phenoxyphenol) can produce compounds with humic-like fluorescence upon direct photolysis (Bianco et al., 2014). These findings suggest that one of the pathways leading to the production of HULIS may be the irradiation and/or the (photo)oxidation of aqueous phenols. This pathway is potentially very interesting in an atmospheric context, where a major competitive process (bacterial degradation of vegetal debris including most notably lignin compounds) is expected to play a less important role compared to surface waters and soil (Valero et al., 2014). It is also consistent with the results of recent studies, according to which the photooxidation of phenolic compounds arising from biomass burning produces potential SOA precursors (Sun et al., 2010; Li et al., 2014; Huang et al., 2018). To get further insight into the possible aqueous-phase photoinduced pathway(s) to atmospheric HULIS, in this work we studied the light-induced transformation of some phenolic compounds typically emitted by biomass burning (Simoneit, 2002). The phototransformation mixtures were

characterized for their light absorption, fluorescence and mass spectrometric properties, with the purpose of detecting the occurrence of compounds with humic-like features. By so doing, we can shed light on both a potential photoinduced pathway to HULIS, and the type of molecular structures that make up this class of compounds.

Experimental

Irradiation experiments

For steady-state irradiation, solutions (10^{-4} mol L^{-1} initial concentration) of the compounds under study (acetosyringone, o-vanillin, syringol, guaiacol, vanillic acid, gallic acid, m-cresol; all of analytical grade, Sigma-Aldrich) were prepared in Milli-Q water. These concentration values were chosen for experimental convenience, to ensure a good monitoring of the different signals to be measured, at the same time avoiding excessively high concentration values that would enhance oligomerization processes. A custom-built double-wall photoreactor made up of borosilicate glass, with a volume of 130 cm^3, was used for the irradiation experiments. Samples were magnetically stirred during irradiation, and the temperature during all the experiments was held at 293 K using a thermostatic bath (LAUDA ECO RE 630 GECO, Germany).

A high-pressure Xenon lamp (500 W) was used as the light source to simulate sunlight irradiation. A water filter was applied to remove infrared radiation, and it was coupled to a cut-off filter at wavelengths 300 nm $\leq \lambda \leq$ 700 nm, to provide UV-Vis radiation that is relevant to the lower boundary layer of the atmosphere. The lamp emission spectrum was measured with a calibrated spectroradiometer (Ocean Optics, USA), equipped with a linear-

array CCD detector. The relevant UV irradiance (30 W m^{-2} in the 290-400 nm wavelength range) is representative of summertime, fair-weather sunlight (Bianco et al., 2014).

All the irradiation experiments were performed in duplicate. The solutions were irradiated for up to 24 h, and 10-mL sample aliquots were withdrawn from the reactor at scheduled time intervals to measure residual substrate concentration, UV-Vis absorption spectra, fluorescence excitation-emission matrices (EEM), as well as mass spectra by ultra-high resolution mass spectrometry. Samples exposed to 24-h irradiation under our constant lamp irradiance conditions receive a fluence analogous to 2-3 days of sunlight exposure (day-night cycle included) in clear-sky, mid-latitude summer (Berto et al., 2016). This is well within the range of the typical atmospheric residence times of aerosols (Balkansky et al., 1993).

Photoinduced transient species were investigated by means of the laser flash photolysis (LFP) technique. For these experiments, the third harmonic of a Nd:YAG laser (λ_{exc} = 355 nm, 85 mJ/pulse) was used at ambient temperature (293 ± 2 K). Experiments were performed in aerated solution or in O_2-sparged (oxygen-saturated) or Ar-sparged (deoxygenated) systems, to investigate the triplet-state reactivity. The absorption evolution at pre-selected wavelengths was followed at each 10 nm from 300 to 600 nm. The absorption decay was then plotted for different wavelengths, to obtain the evolution of the transient spectrum as a function of time. Further information concerning the LFP experimental set-up is reported elsewhere (De Laurentiis et al., 2013a and b).

Characterization of the irradiated solutions

The time trend of the concentration of the irradiated substrates was monitored by means of high performance liquid chromatography with diode array detection (HPLC-DAD), using a VWR-Hitachi Elite LaChrom instrument equipped with L2455 diode array detector, L2130

quaternary pump module, L2300 column oven (set at 40°C), L2200 autosampler (sample injection volume 60 µL), Duratec vacuum degasser and a reverse-phase column Merck LiChroCART packed with LiChrospher 100 RP18 (125 mm × 4 mm × 5 µm).

The absorption spectra of the solutions before and after irradiation were taken with a Varian Cary 100 Scan double-beam UV-Vis spectrophotometer, using Hellma quartz cuvettes with 1 cm optical path length. The absorption spectra (molar absorption coefficients) of the studied compounds before irradiation are reported in **Figure SM1** in the Supplementary Material (hereafter SM). The EEM spectra were measured with a VARIAN Cary Eclipse Fluorescence Spectrophotometer, with an excitation range from 200 to 400 nm at 10 nm steps, and an emission range from 200 to 600 nm with a scan rate of 1200 nm min^{-1}. Excitation and emission slits were set at 10 nm. The solutions during spectra measurements were contained in a fluorescence quartz cuvette (Hellma) with 1 cm optical path length. The Raman signal of water was taken as a reference for lamp intensity and signal stability within different measurements.

The samples were also characterized by Fourier transform-ion cyclotron resonance mass spectrometry (FT-ICR-MS). This technique, with ultrahigh resolution and ppb mass accuracy of its spectra, allows for a confident assignment of a unique elemental composition for each mass spectrum peak (Kew et al., 2017). It is one of the most powerful tools used for the characterization of complex organic compounds in ambient aerosols at the molecular level (Altieri et al., 2008; Jiang et al., 2016). A solariX XR FT-ICR-MS instrument was used (Bruker Daltonik GmbH, Bremen, Germany), equipped with a refrigerated, 9.4 T actively shielded superconducting magnet (Bruker Biospin, Wissembourg, France) and a Paracell analyzer cell. The ESI ion source (Bruker Daltonik GmbH, Bremen, Germany) was operated in the negative mode. The detection mass range was set to m/z 150 – 1000, and ion accumulation time to 0.65 s. A total of 64 continuous 4M data FT-ICR transients were co-

added to enhance the signal-to-noise ratio and dynamic range. The mass spectra were calibrated externally with arginine clusters in negative ion mode, using a linear calibration. The final spectra were internally recalibrated with typical O_2 class species peaks using quadratic calibration in DataAnalysis 4.4 (Bruker Daltonics). A typical mass-resolving power (m/Δm50%, where Δm50% is the mass spectral peak full width at half-maximum peak height) >450 000 was achieved at m/z 319, with <0.3 ppm absolute mass error.

The custom software was used to calculate all mathematically possible formulas for all ions with a signal-to-noise ratio above 10, using a mass tolerance of ±1ppm. The maximum number of atoms for the formula calculator was set to: 30 ^{12}C, 60 ^{1}H, 20 ^{16}O, 3 ^{14}N, 1 ^{32}S, 1 ^{13}C, 1 ^{18}O and 1 ^{34}S. For the chemical formula $C_cH_hO_oN_nS_s$, the double-bond equivalent (DBE) is calculated using the following equation: DBE = (2c+2−h+n)/2. The details of data processing have been described previously (Shi et al., 2012; Jiang et al., 2014).

Results and Discussion

Time evolution of substrate concentration and of absorption (UV-Vis) and fluorescence (EEM) spectra

Irradiation results for the biomass-burning compounds under study are reported in **Figure 1**, showing the following photoreactivity order: acetosyringone (AcS) > o-vanillin (VN) > vanillic acid (VA) > guaiacol (GUA) > m-cresol (CRE). The photoreactivity trend roughly matched the average values of the molar absorption coefficients above 300 nm, which were the highest for AcS and VN, intermediate for VA, and very low and similar for GUA and CRE (see SM, **Figure SM1**). Moreover, syringol behaved similarly to CRE and gallic acid to

VA (these data are not shown on the plot for readability issues; the time trends of syringol and gallic acid are reported in **Figure SM2** in the SM). Note that no transformation was detected in dark controls, thereby excluding hydrolysis and similar processes. Interestingly, the most photoactive compounds (AcS and VN) were those bearing a carbonyl group in addition to the phenolic one.

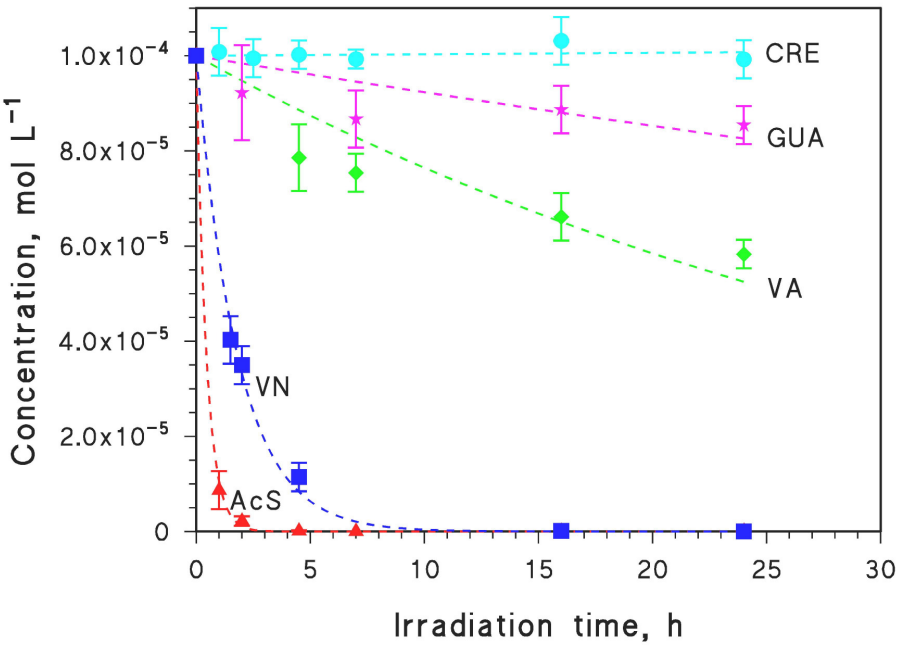

Figure 1. Time trends of the studied compounds under simulated sunlight irradiation. AcS: acetosyringone; VN: o-vanillin; VA: vanillic acid; GUA: guaiacol; CRE: m-cresol. The error bars represent the standard error of replicate measurements. Note that the gallic acid data points (not shown here) almost coincided with those of VA, and a similar issue holds for CRE and syringol.

Overall, new fluorescence signals that could be assigned to humic-like species were only detected in the cases of irradiated AcS and VN. After 24-h irradiation time AcS and VN no longer occurred in solution (**Figure 1**), but in both irradiated systems two new fluorescence peaks could be noticed at excitation(Ex)/emission(Em) wavelengths, Ex/Em = 200/400 nm

and 300/400 nm (**Figure 2**). These signals correspond to the spectral regions of peak A and peak C of humic substances (Coble, 1996), and the relevant EEM spectra agree well with the fluorescence properties of HULIS (Fan et al., 2016; Han and Kim, 2017). AcS and VN underwent rather fast phototransformation (**Figure 1**). At the same time one can notice a quick loss of the absorbance features of the initial substrates (**Figure 3**), in particular as far as the AcS absorption peak at around 300 nm and the VN peaks at 240, 280 and 320 nm are concerned. The overall shape of the absorption spectra also changed, with an increase in the solution absorbance in the long UVA (370-400 nm) and visible regions (**Figure 3**).

In the cases of VA, GUA, CRE, gallic acid and syringol, no new fluorescence peaks appeared (see SM, **Figure SM3**), and the absorption spectra did not change noticeably as a function of the irradiation time, at least up to 24 h irradiation. As far as CRE and syringol are concerned, this result is easily explained by poor photochemical transformation. In the cases of VA, GUA and gallic acid, the stability over time of the absorption spectra despite the occurrence of some degradation suggests that the transformation intermediates had similar absorption properties as the initial substrates. From a molecular structure point of view, the main difference between these compounds and AcS/VN is that AcS and VN are the only compounds bearing both a phenolic and a carbonylic group (vide infra).

A similar phenomenon as that observed for AcS and VN (absorbance increase above 350 nm, appearance of humic-like fluorescence bands in the forms of A and C peaks) has already been observed during the photosensitized oxidation of phenol and 4-phenoxyphenol (De Laurentiis et al., 2013a/b), as well as the direct photolysis of tyrosine and 4-phenoxyphenol (Bianco et al., 2014). In those previous studies, evidence has been found of the formation of dimers of the initial substrates. Moreover, quantum mechanical calculations have shown that if the process goes on and oligomers are formed, they are very likely to emit fluorescence radiation at around 400 nm (Barsotti et al., 2016).

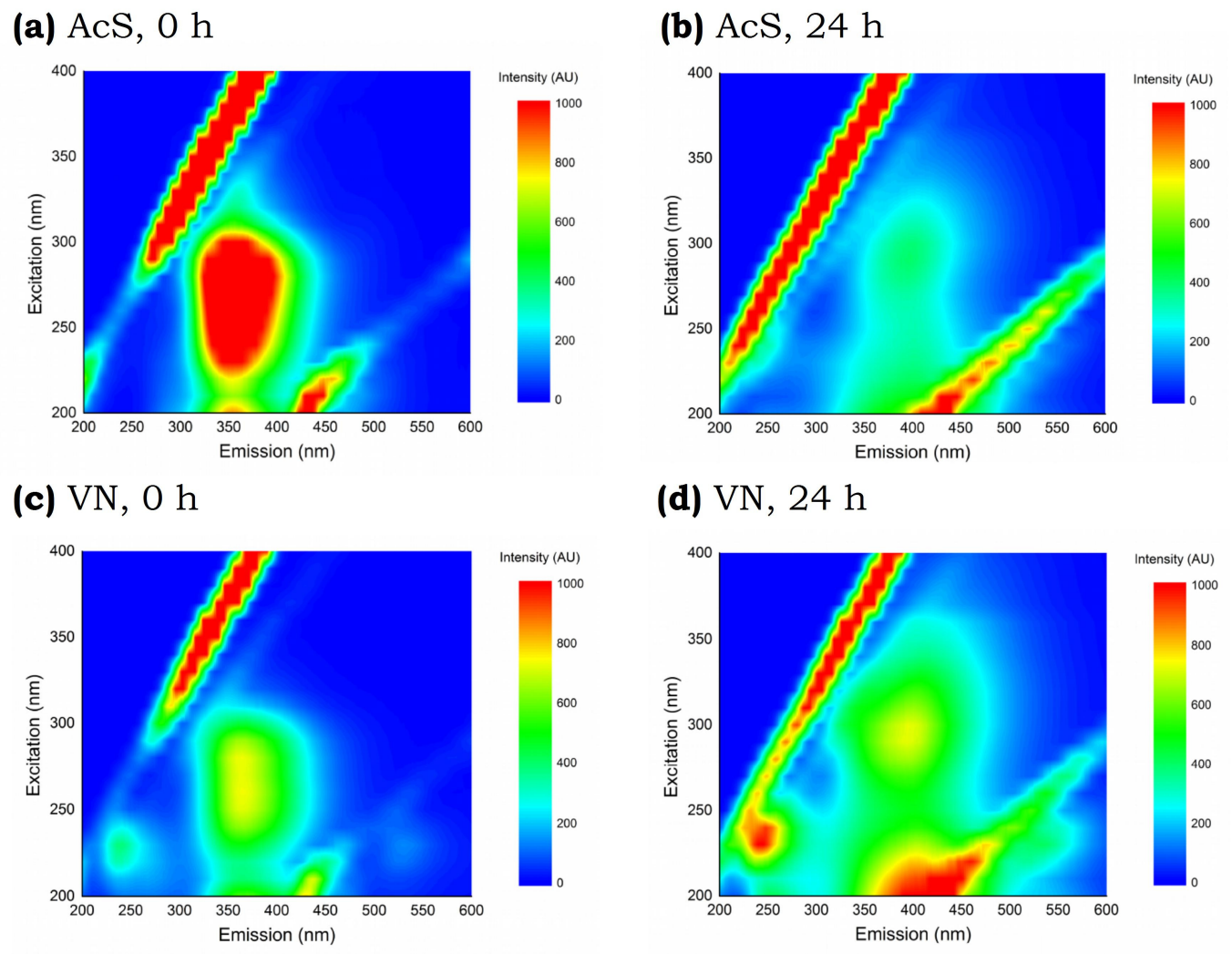

Figure 2. Excitation-emission matrix (EEM) spectra of AcS and VN, before and after 24-h irradiation. **(a)** AcS, before irradiation; **(b)** AcS, 24 h irradiation; **(c)** VN, before irradiation; **(d)** VN, 24 h irradiation. Bands with Em ~ 400 nm already appeared after 8 h irradiation of AcS and 16 h irradiation of VN.

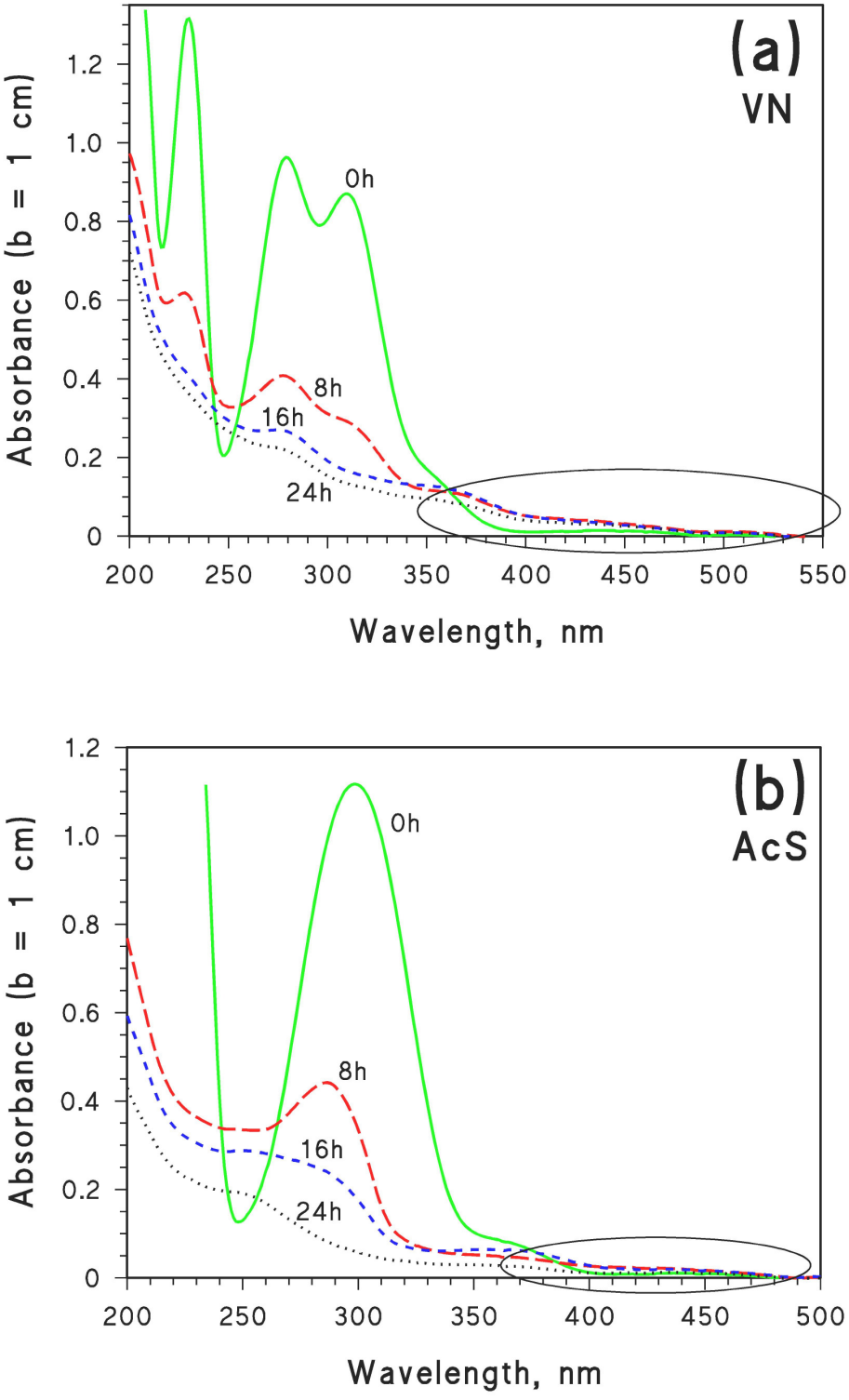

Figure 3. Time trends of the absorption spectra of **(a)** AcS and **(b)** VN under irradiation (for 0, 8, 16 and 24 hours). The ellipses highlight the UVA-Vis spectral ranges where the absorbance increased with irradiation ($\lambda > 370$ nm for VN, $\lambda > 390$ nm for AcS).

The studied compounds that produced HULIS-type fluorescence when irradiated (AcS and VN) were the only ones to bear both a phenolic group (-OH) and an aromatic carbonyl (-CHO for VN, -$COCH_3$ for AcS). Irradiated carbonyls can undergo a Norrish-type pathway, with H abstraction from -CHO and CH_3 abstraction from -$COCH_3$ (Paulson et al., 2006). The phenolic groups can be turned into phenoxy radicals (Net et al. 2009), which can undergo condensation pathways (Berto et al., 2016). The Norrish reaction stems from triplet states, while phenoxyls can derive either from photoinduced O-H bond breaking, or from oxidation of ground-state molecules by excited triplets (De Laurentiis et al., 2013a; Berto et al., 2016). Therefore, it is important to understand the nature of the AcS and VN excited states.

Laser flash photolysis (LFP) results

To elucidate the possible processes involving light-excited AcS and VN, we studied the nature of their excited states and the relevant reactivity by means of LFP, which is a very useful technique to study the properties of short-lived transients (Windsor, 2003). **Figure 4** shows the time-dependence decay of the transient spectrum after the laser pulse of VN (2.86 mM) and AcS (1.47 mM) solutions in Milli-Q water. For VN, the main transient peak was centered at 370 nm and its decay followed pseudo-first order kinetics (k' ~ 1.86×10^6 s^{-1} in aerated solution). The decay kinetics of this species was directly correlated to the oxygen concentration in solution (**Figure 5a**), suggesting that a triplet state of VN (^{3}VN*) was generated after the laser pulse. Excited triplet states are well known to react with dissolved oxygen to produce either inactivation or $^1O_2$ generation (Gorman et al., 1984). In **Figure 4** it is interesting to notice that the 370-nm (^{3}VN*) signal completely disappeared after 2.0 μs, while a new transient appeared with absorption maximum between 380 and 440 nm, i.e., with similar features as previously reported phenoxy radicals (Tang et al., 2012). The rate constant

of triplet-state decay was directly proportional to the VN concentration (**Figure 5b**), which suggests a reaction between ^{3}VN* and ground-state VN. In the presence of phenolic compounds, these reactions usually produce phenoxy radicals because the triplet state oxidizes the ground-state phenol (De Laurentiis et al., 2013a/b).

In the case of AcS, it was observed the formation and decay of a transient species with absorption maximum at 355 nm. Similarly to the case of VN, the decay rate constant of this 355-nm transient increased with dissolved oxygen concentration (**Figure 5a**), suggesting that the transient is likely to be the AcS triplet state (^{3}AcS*). Note that the oxygen concentration was varied by purging the solutions with Ar or O_2, or by leaving them in equilibrium with air. The latter case ($[O_2] \sim 3\times10^{-4}$ M) is representative of air-equilibrated atmospheric aerosols. Moreover, the ^{3}AcS* decay rate constant increased with increasing AcS concentration (**Figure 5b**), which suggests as well the possibility of a reaction between ^{3}AcS* and ground-state AcS. Some radiation absorption in the range of 410-440 nm (**Figure 4**) might be consistent with the occurrence of a phenoxy radical, although with lower absorption compared to the case of VN. Assuming that the notation RCO-Ph-OH represents either VN or AcS that bear both a carbonyl and a phenoxyl group, reactions (1-2) may be hypothesized based on the laser flash photolysis results (ISC = inter-system crossing, ^{3}RCO-Ph-OH* is a triplet state, RCO-Ph-O$^\bullet$ a phenoxy radical). Moreover, reaction (3) may occur as well under irradiation conditions (Berto et al., 2016). The formation of triplet states and phenoxy radicals enables both the Norrish-type reactions and the phenoxyl condensation pathways.

$$\text{RCO-Ph-OH} + h\nu \xrightarrow{ISC} {}^3\text{RCO-Ph-OH}^* \qquad (1)$$

$$^3\text{RCO-Ph-OH}^* + \text{RCO-Ph-OH} \rightarrow \text{RC}^\bullet\text{OH-Ph-OH} + \text{RCO-Ph-O}^\bullet \qquad (2)$$

$$\text{RCO-Ph-OH} + h\nu \rightarrow \text{RCO-Ph-O}^\bullet + \text{H}^\bullet \qquad (3)$$

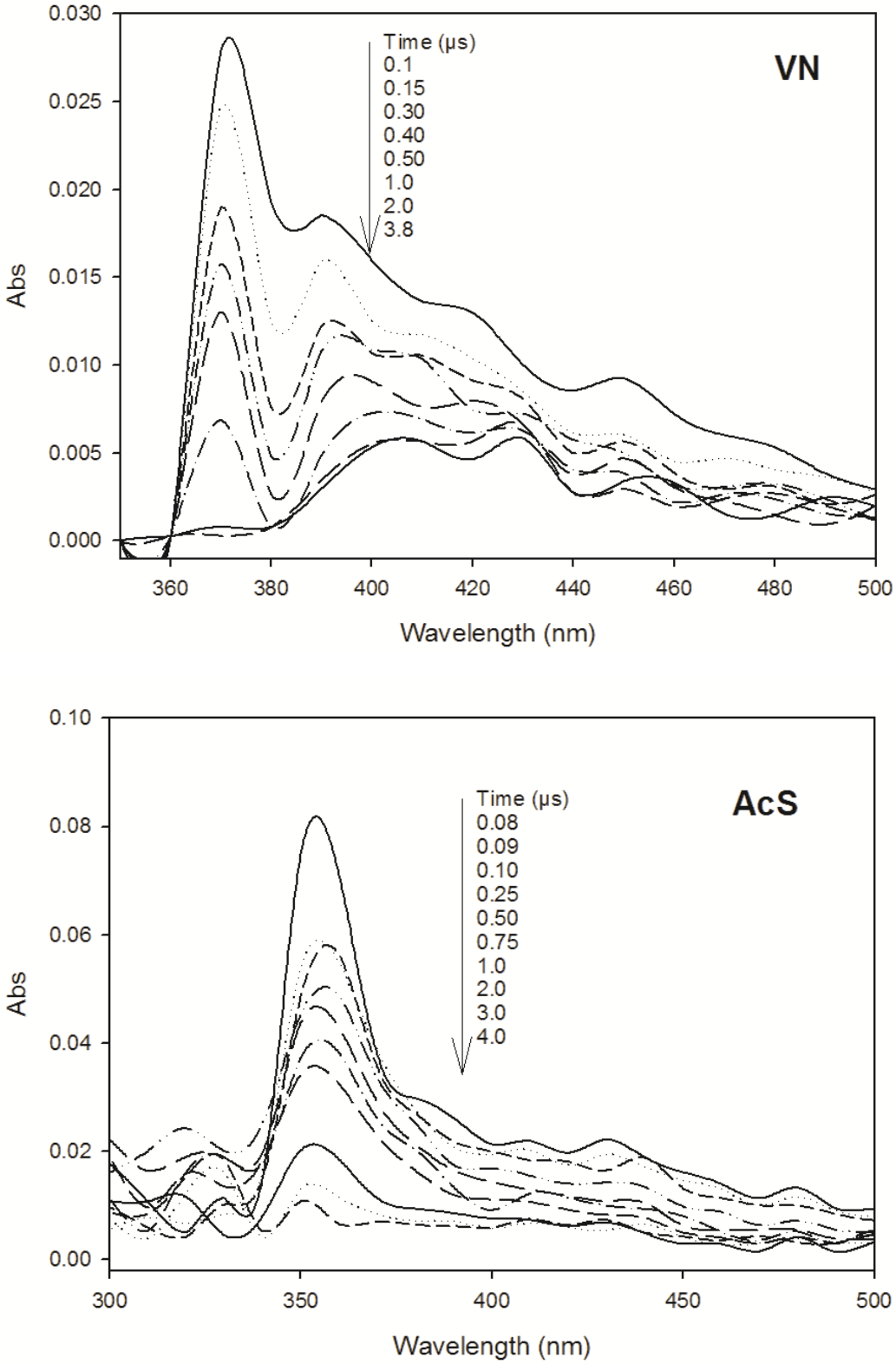

Figure 4. Transient spectra obtained upon laser irradiation (λ_{exc} = 355 nm, 85 mJ/pulse) in aerated solution of 2.86 mM VN (top) and 1.47 mM AcS (bottom). The time corresponding to each spectrum is shown as a legend on the figure.

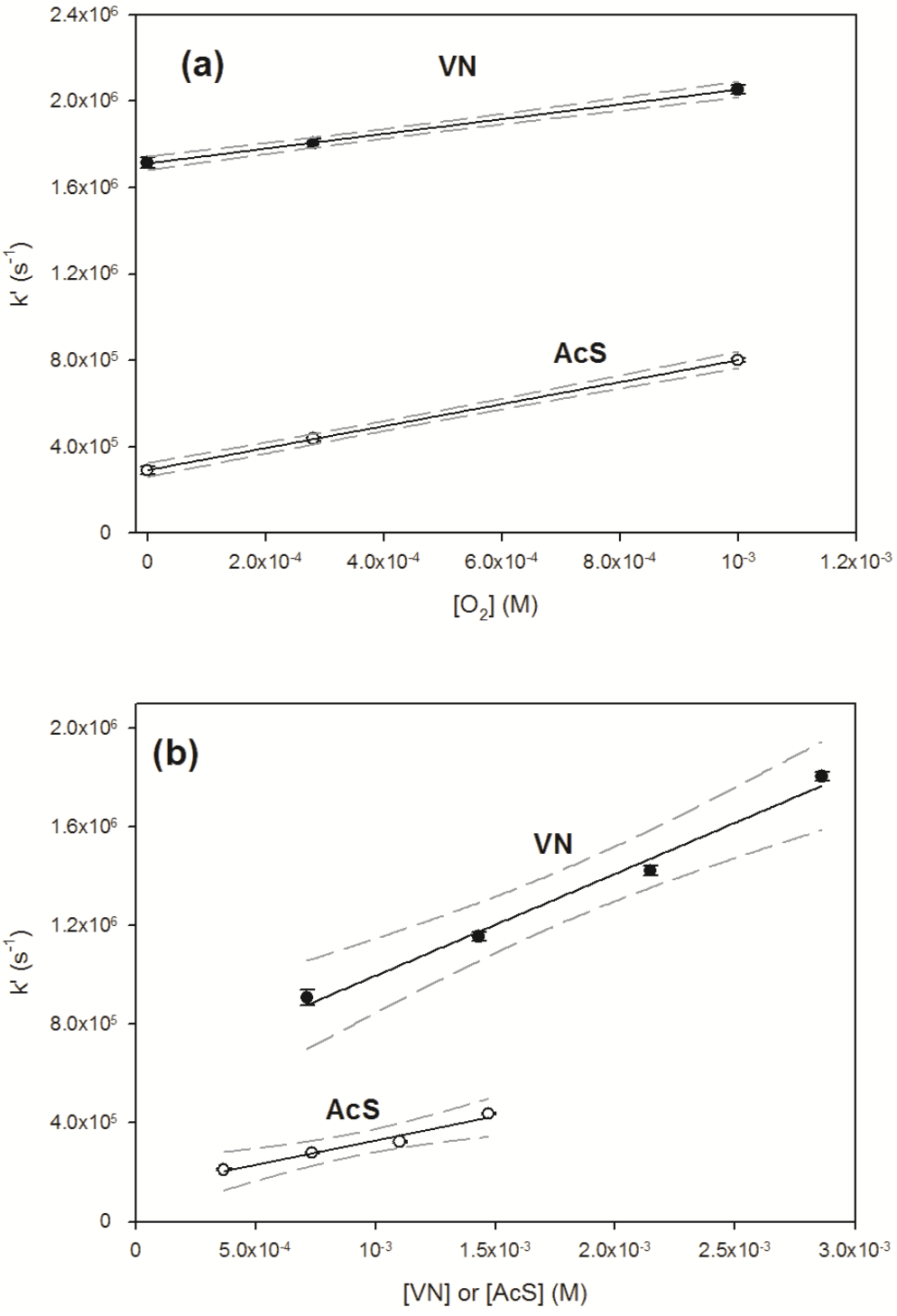

Figure 5. (a) Trends of the decay constants of the transient signals at 370 nm (VN) and 355 nm (AcS) as a function of the concentration of dissolved oxygen, derived from O_2 water solubility data (Franco and Olmsted, 1990). **(b)** Trends of the decay constants of the same signals, as a function of substrate concentration (VN or AcS). Laser irradiation in all the cases: λ_{exc} = 355 nm, 85 mJ/pulse.

Chemical characterization by ultra-high resolution mass spectrometry

The possible formation (or lack of formation) of oligomeric species, and so possible HULIS candidates, during the photodegradation of AcS and VN was studied by using FT-ICR-MS. Interestingly, AcS and VN yielded humic-like fluorescence upon irradiation and they also produced oligomeric species (vide infra). By contrast, no formation of oligomers was detected in the cases of VA and GUA under irradiation at the same time scale, which combined with the lack of humic-like fluorescence in the respective irradiated samples despite the occurrence of some photodegradation. The relative abundance of measured ions before and after irradiation of AcS, VN, VA and GUA is shown in the SM (see **Figures SM4-SM7**).

The complex mass spectrum obtained by ultra-high-resolution FT-ICR-MS can be simplified by the Van Krevelen diagram (Reinhardt et al., 2007, Wang et al., 2017, Schurman et al., 2018), obtained by plotting the H/C ratio against the O/C ratio for individual assigned atomic formulas of the products. The Van Krevelen diagrams of VN and AcS are reported in **Figures 6a** and **6b**, respectively. Plotting the Kendrick mass defects (KMD) against the Kendrick nominal masses, all the species that belong to the same homologous series align on the same horizontal line (Kew et al., 2017).

In the case of VN we calculated the KMD of $C_8H_8O_3$ for all the formulas, to find the compounds that differ by this mass subunit. Twelve series were identified in this way, which show a convergence point with O/C = 0.375 and H/C = 1.

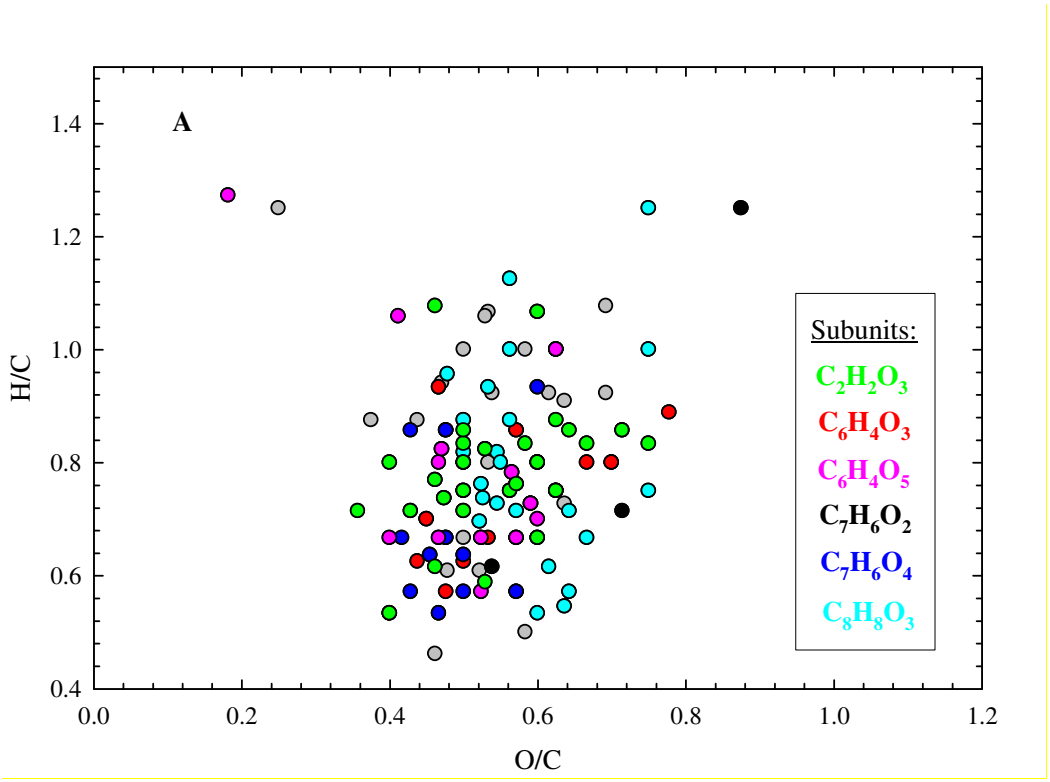

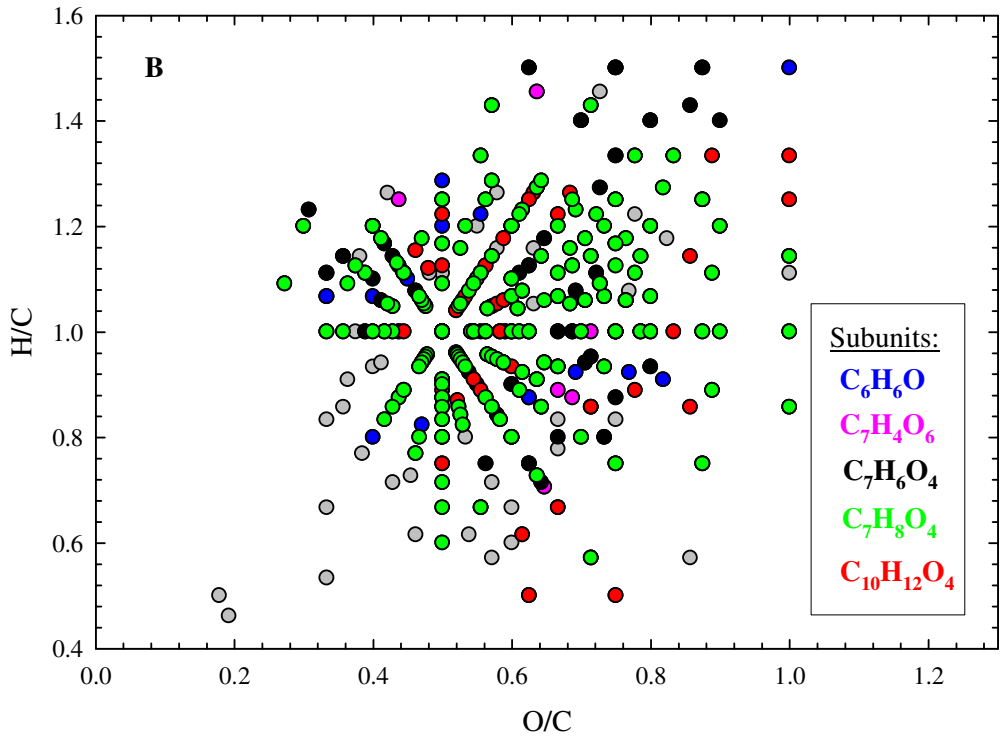

Figure 6. Van Krevelen plot of $C_xH_yO_z$-compounds emerged upon 24 hours irradiation of **(A)** VN and **(B)** AcS. The six (A) and five (B) chemical block increments are denoted by the different symbols labeled in the legend.

Eleven homologous series were also identified with the mass increment of $C_7H_6O_4$, which has a convergence point of O/C = 0.57 and H/C = 0.86. In this case the identified compounds derived from VN photodegradation are separated by the regular mass m/z 154, resulting in an increase of the molecular weight and double-bond equivalent (DBE). **Scheme 1** tentatively accounts for the observed molecular formulas $C_{15}H_{12}O_7$ ($C_7H_6O_4$ addition to VN) and $C_{16}H_{14}O_6$ ($C_8H_8O_3$ addition). Such increases in the molecular mass can be accounted for in the framework of the condensation between two phenoxyl radicals or between a phenoxyl and a ketyl radical, the latter deriving from a Norrish-type process (Paulson et al., 2006). However, additional reaction pathways such as demethylation (-OCH_3 → -OH) and aldehyde oxidation (-CHO → -COOH) should also be hypothesized to obtain the mass increase corresponding to $C_7H_6O_4$. These additional pathways are often observed in direct photolysis processes (Bustos et al., 2019). Further chemical building block increments ($C_2H_2O_3$, $C_6H_4O_3$, $C_6H_4O_5$, $C_7H_6O_2$) were identified (**Figure 6A**), which also result in an increase of molecular mass and DBE with formation of oligomers. The processes behind those increments could additionally involve demethylation, oxidation/hydroxylation processes, as well as fragmentation of the aromatic ring.

Regarding the oligomers formed by AcS photodegradation, seventeen series were identified separated by the mass subunit $C_{10}H_{12}O_4$, which corresponds to the AcS molecular mass (m/z 196). The convergence point of the oligomer series has O/C = 0.4 and H/C = 1.2. Seventy-six homologous series were identified and separated by the mass subunit $C_7H_8O_4$ (m/z 156). The convergence point for this oligomer series has O/C = 0.57 and H/C = 1.1. In both identified series most compounds have an H/C ratio lower than 1.2, which is the H/C ratio of AcS, indicating photooxidation reactions.

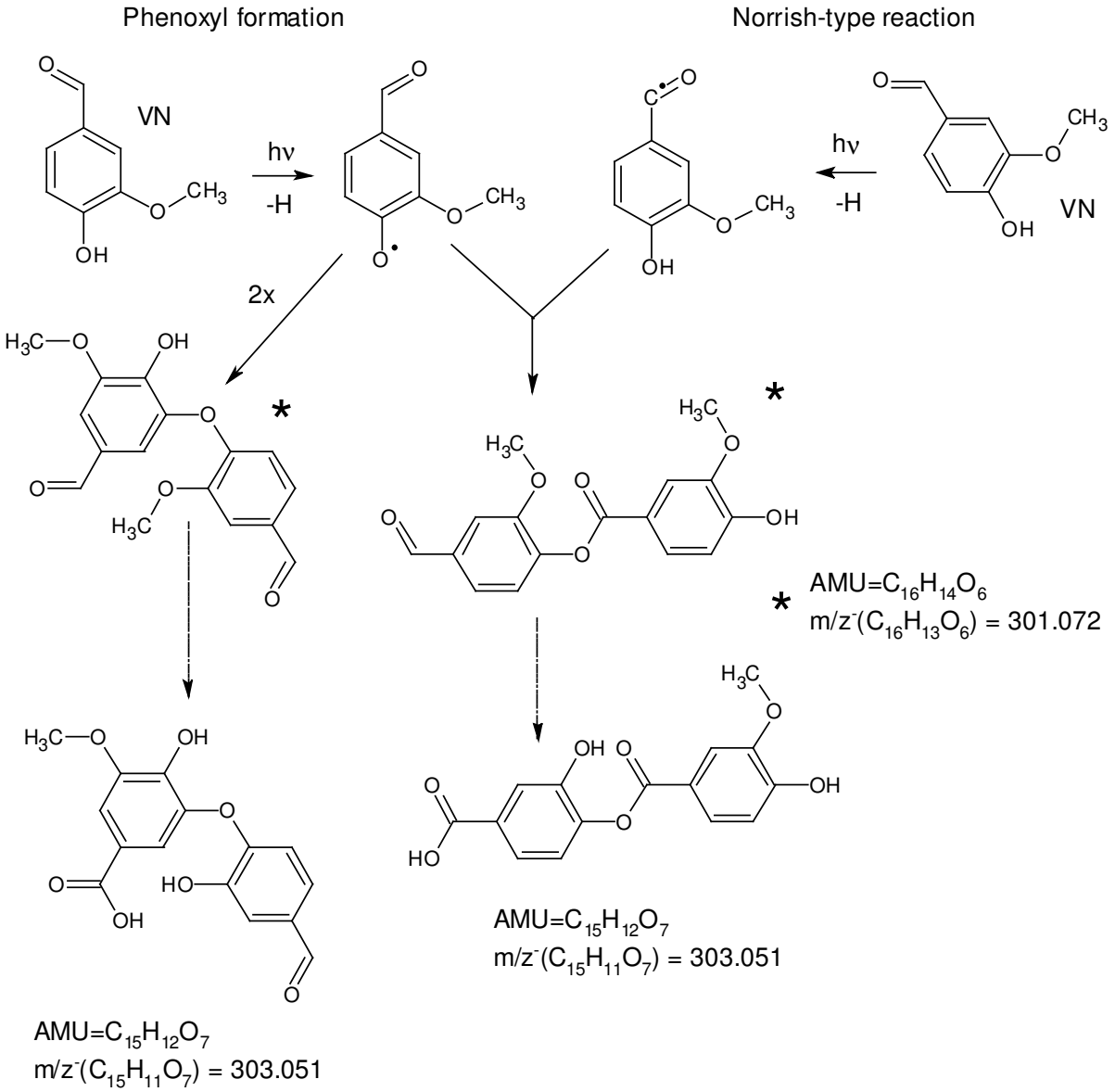

Scheme 1. Proposed (tentative) reaction pathways from the photolysis of o-vanillin (VN), leading to the detected compound(s) with formulas $C_{16}H_{14}O_6$ and $C_{15}H_{12}O_7$, based on phenoxyl and Norrish-type reactions. The dashed arrows represent additional processes that combine demethylation ($-OCH_3 \rightarrow -OH$) with oxidation of the aldehyde group ($-CHO \rightarrow -COOH$). The phenoxy radical can also be formed upon oxidation of ground-state VN by ^{3}VN* (process not shown for scheme readability issues).

We found that the oligomerization process also involved the repeating building-block increments C_6H_6O, $C_7H_4O_6$, $C_7H_6O_4$ and $C_{10}H_{12}O_4$ (see **Figure 6B**). The latter increment implies dimerization, while the others would also require fragmentations (e.g., demethylation) and oxidation. **Scheme 2** reports a tentative reaction pathway that might account for the formation of one of the most intense peaks ($C_{16}H_{16}O_8$), always based on phenoxyl and Norrish-type reactions. Additional reactions such as demethylation ($-OCH_3 \rightarrow -OH$) should again be hypothesized to obtain the observed mass increment.

It has been demonstrated that the iso-abundance plots of double bond equivalent (DBE) versus carbon numbers can be a useful tool for the differentiation of complex organic mixtures based on the chemical composition (Jiang et al., 2014; Mekic et al. 2018). The iso-abundance plot of DBE *versus* carbon numbers for the detected $C_xH_yO_z$ species in this work is presented in **Figure 7**.

DBE is the number of double bonds plus rings representing unsaturations, and **Figure 7** shows a linear increase of DBE with increasing number of carbon atoms in the reaction products. The case of VN is shown in **Figure 7a** and the corresponding DBE values ranged between 5 and 17, with 8-23 carbon atoms and 6-22 oxygen atoms. Three distinctive regions can be recognized in **Figure 7a**, corresponding to monomers (C_5-C_8), dimers (C_9-C_{13}) and trimers (C_{14}-C_{17}).

Figure 7b (AcS photodegradation) indicates that most of the $C_xH_yO_z$ products formed from AcS exhibit DBE values in the range between 4 and 14, with 6-26 carbon atoms. As suggested in **Scheme 2**, formation of dimeric species from AcS would take place along with the loss of some carbon atoms in demethylation processes, and similar phenomena would likely occur in trimer formation as well. Moreover, because AcS (a C_{10} compound) might also lose some subunits upon irradiation to produce lighter species, some of the identified compounds may well be dimers and trimers of the latter.

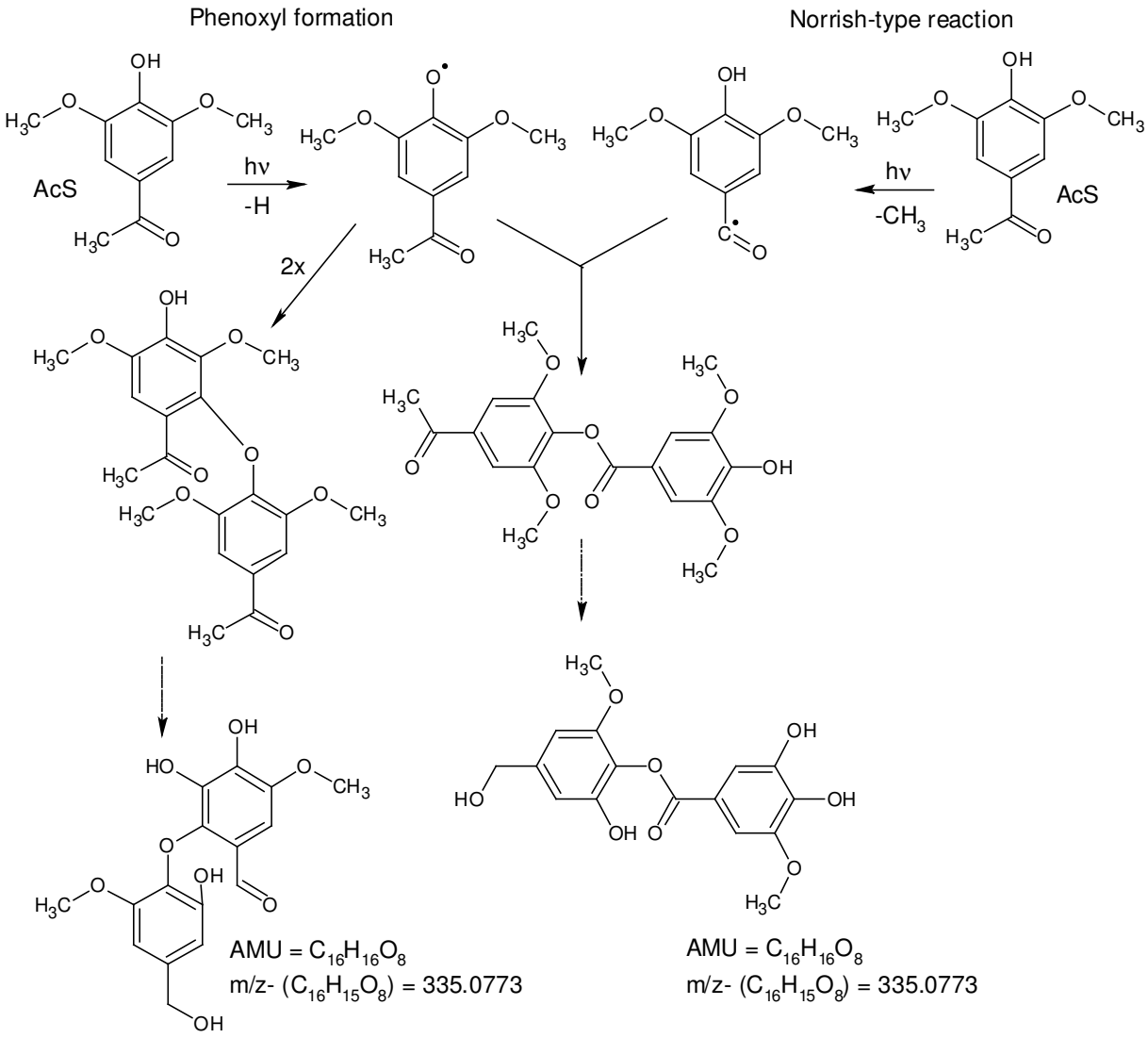

Scheme 2. Proposed (tentative) reaction pathways from the photolysis of acetosyringone (AcS), leading to the detected compound(s) with formula $C_{16}H_{16}O_8$, based on phenoxyl and Norrish-type reactions. The dashed arrows represent processes that combine demethylation pathways with reduction of the aldehyde group. The phenoxy radical can also be formed upon oxidation of ground-state AcS by ^{3}AcS* (not shown here for scheme readability issues).

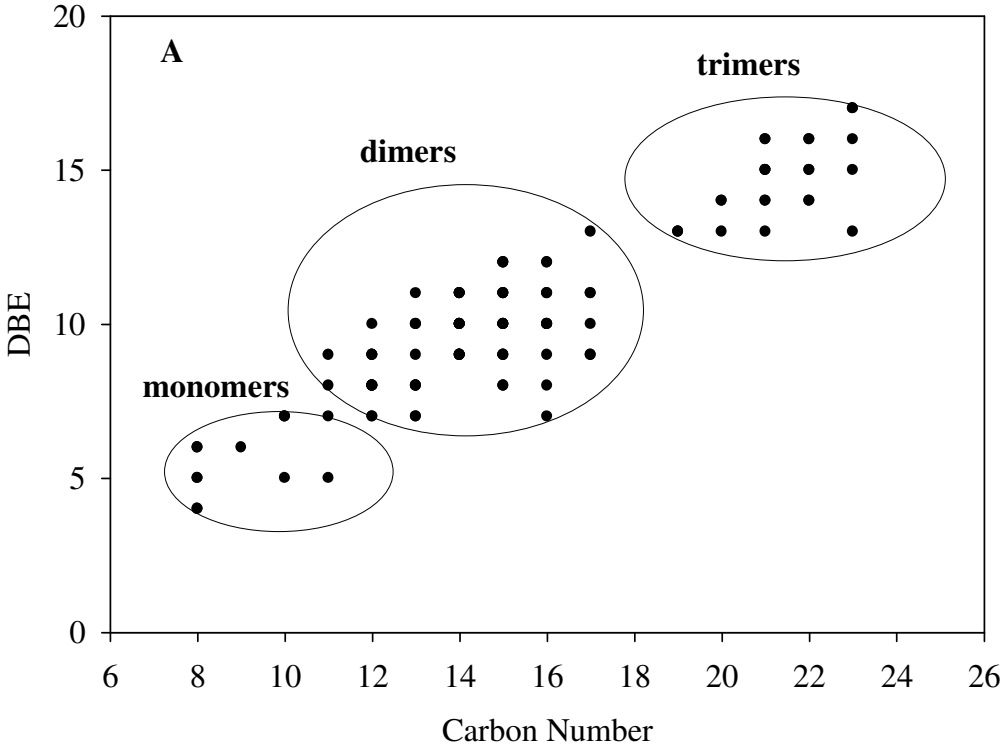

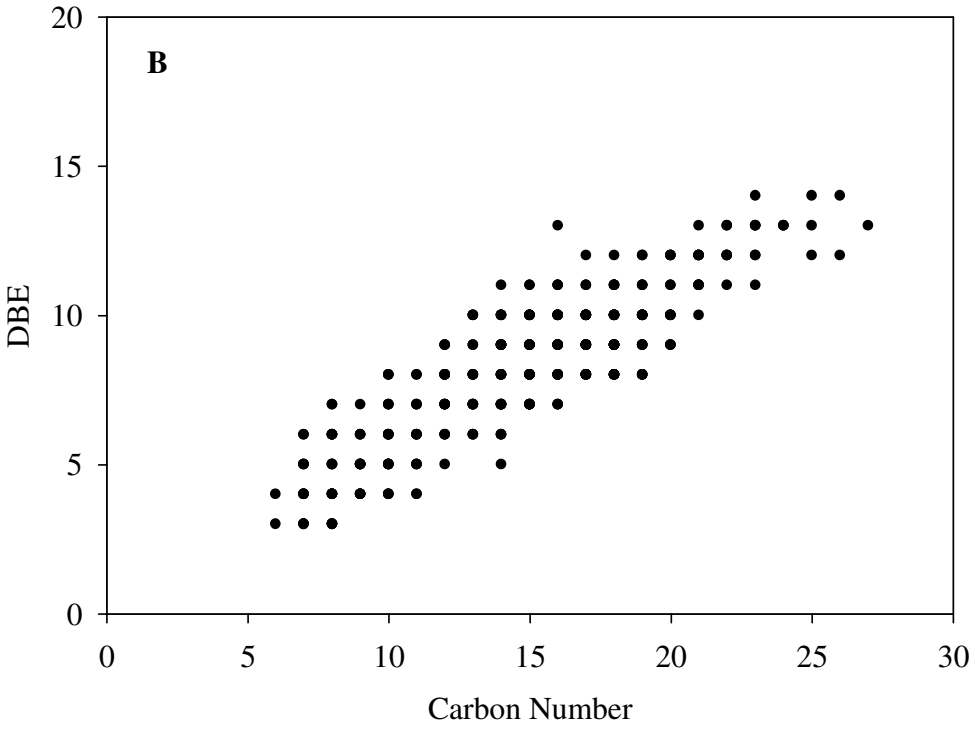

Figure 7. Iso-abundance plot of DBE *versus* carbon numbers for the $C_xH_yO_z$ species detected upon 24-h irradiation of **(A)** VN and **(B)** AcS.

Conclusions

The irradiation of o-vanillin and acetosyringone under simulated sunlight was here shown to produce intermediates with humic-like fluorescence. The reaction intermediates had also higher absorption than the parent compounds above 370-390 nm. The characterization of the irradiated samples by FT-ICR-MS showed the occurrence of species that could be interpreted as dimers and trimers of the parent compounds and/or their early transformation intermediates.

In contrast, no evidence of the formation of HULIS species was obtained upon irradiation of other investigated phenolic compounds (m-cresol, vanillic acid, guaiacol, syringol, gallic acid). Our findings suggest that there might be a link between oligomerization and some properties that are observed in irradiated solutions, such as the occurrence of humic-like fluorescence and the increase of absorption in the long-wavelength UVA and visible spectral range. These findings are consistent with quantum mechanical predictions of the possible fluorescence properties of phenol oligomers (Barsotti et al., 2016).

Based on the present results, we can conclude that derivatives possessing the main properties attributed to atmospheric humic-like substances (HULIS) may be formed upon sunlight irradiation of some phenolic compounds that are commonly emitted by biomass burning. Therefore, a photoinduced pathway to HULIS formation from low molecular weight compounds might take place in the atmosphere, in the presence of a liquid phase or of a water layer surrounding deliquescent particles.

Acknowledgements

DV acknowledges financial support by MIUR-PNRA. This work has been also supported by the French Ministry of Environment.

References

Altieri, K. E., Seitzinger, S. P., Carlton, A. G., Turpin, B. J., Klein, G. C., Marshall, A. G., 2008. Oligomers formed through in-cloud methylglyoxal reactions: Chemical composition, properties, and mechanisms investigated by ultra-high-resolution FT-ICR mass spectrometry. Atmos. Environ. 42, 1476-1490.

Balkansky, Y. J., Jacob, D. J., Gardner, G. M., Graustein, W. C., Turekian, K. K., 1993. Transport and residence times of atmospheric aerosols inferred from a global three-dimensional simulation of ^{210}Pb. J. Geophys. Res. 98, 20573-20586.

Barsotti, F., Ghigo, G., Vione, D., 2016. Computational assessment of the fluorescence emission of phenol oligomers: A possible insight into the fluorescence properties of humic-like substances (HULIS). J. Photochem. Photobiol. A: Chem. 315, 87-93.

Berto, S., De Laurentiis, E., Tota, T., Chiavazza, E., Daniele, P.G., Minella, M., Isaia, M., Brigante, M., Vione, D., 2016. Properties of the humic-like material arising from the photo-transformation of L-tyrosine. Sci. Total Environ. 545-546, 434-444.

Bianco, A., Minella, M., De Laurentiis, E., Maurino, V., Minero, C., Vione, D., 2014. Photochemical generation of photoactive compounds with fulvic-like and humic-like fluorescence in aqueous solution. Chemosphere 111, 529-536.

Boucher, O., Randall, D., Artaxo, P., Bretherton, C., Feingold, G., Forster, P., Kerminen, V.-M., Kondo, Y., Liao, H., Lohmann, U., 2013. Clouds and Aerosols. Climate Change

2013: The Physical Science Basis. Contribution of Working Group I to the Fifth Assessment Report of the Intergovernmental Panel on Climate Change. Cambridge University Press, pp. 571–657.

Bustos, N., Cruz-Alcalde, A., Iriel, A., Cirelli, A. F., Sans, C., 2019. Sunlight and UVC-254 irradiation induced photodegradation of organophosphorus pesticide dichlorvos in aqueous matrices. Sci. Total Environ. 649, 592-600.

Chan, M. N., Chan, C. K., 2003. Hygroscopic properties of two model humic-like substances and their mixtures with inorganics of atmospheric importance. Environ. Sci. Technol. 37, 5109-5115.

Chang, J. L., Thompson, J. E., 2010. Characterization of colored products formed during irradiation of aqueous solutions containing H_2O_2 and phenolic compounds. Atmos. Environ. 44, 541–551,

Coble, P. G., 1996. Characterization of marine and terrestrial DOM in seawater using excitation–emission spectroscopy. Mar. Chem. 51, 325–346.

De Laurentiis, E., Sur, B., Pazzi, M., Maurino, V., Minero, C., Mailhot, G., Brigante, M., Vione, D., 2013a. Phenol transformation and dimerisation, photosensitised by the triplet state of 1-nitronaphthalene: A possible pathway to humic-like substances (HULIS) in atmospheric waters. Atmos. Environ. 70, 318-327.

De Laurentiis, E., Socorro, J., Vione, D., Quivet, E., Brigante, M., Mailhot, G., Wortham, H., Gligorovski, S., 2013b. Phototransformation of 4-phenoxyphenol sensitised by 4-carboxybenzophenone: Evidence of new photochemical pathways in the bulk aqueous phase and on the surface of aerosol deliquescent particles. Atmos. Environ. 81, 569-578.

Dockery, D. W., Schwartz, J., Spengler, J. D., 1992. Air pollution and daily mortality: Associations with particulates and acid aerosols. Environmental Res. 59, 362-373.

Fan, X., Wei, S., Zhu, M., Song, J., Peng, P., 2016. Comprehensive characterization of humic-like substances in smoke $PM_{2.5}$ emitted from the combustion of biomass materials and fossil fuels. Atmos. Chem. Phys. 16, 13321-13340.

Franco, C., Olmsted, J., 1990. Photochemical determination of the solubility of oxygen in various media. Talanta 37, 905-909.

Gorman, A. A., Hamblett, I., Rodgers, M. A. J., 1984. Time-resolved luminescence measurements of triplet-sensitized singlet-oxygen production: variation in energy-transfer efficiencies. J. Am. Chem. Soc. 106, 4679-4682.

Graber, E. R., Rudich, Y., 2006. Atmospheric HULIS: How humic-like are they? A comprehensive and critical review. Atmos. Chem. Phys. 6, 729-753.

Han, H., Kim, G., 2017. Significant seasonal change in optical properties by atmospheric humic-like substances (HULIS) in water-soluble organic carbon aerosols. Atmos. Chem. Phys. Discuss., article #554.

Heal, M.R., Kumar, P., Harrison, R.M., 2012. Particles, air quality, policy and health. Chem. Soc. Rev. 41, 6606–6630.

Huang, D. D., Zhang, Q., Cheung, H. H. Y., Yu, L., Zhou, S., Anastasio, C., Smith, J. D., Chan, C. K., 2018. Formation and evolution of aqSOA from aqueous-phase reactions of phenolic carbonyls: comparison between ammonium sulfate and ammonium nitrate solutions. Environ. Sci. Technol. 52, 9215-9224.

Jiang, B., Liang, Y., Xu, C., Zhang, J., Hu, M., Shi, Q., 2014. Polycyclic aromatic hydrocarbons (PAHs) in ambient aerosols from Beijing: Characterization of low

volatile PAHs by positive-ion atmospheric pressure photoionization (APPI) coupled with Fourier Transform Ion Cyclotron Resonance. Environ. Sci. Technol. 48, 4716-4723.

Jiang, B., Kuang, B. Y., Liang, Y., Zhang, J., Huang, X. H. H., Xu, C., Yu, J. Z., Shi, Q., 2016. Molecular composition of urban organic aerosols on clear and hazy days in Beijing: a comparative study using FT-ICR MS. Environ. Chem. 13, 888-901.

Kew, W., Blackburn, J. W. T., Clarke, D. J., Uhrin, D, 2017. Interactive van Krevelen diagrams - Advanced visualization of mass spectrometry data of complex mixtures. Rapid Commun. Mass Spectrom. 31, 658-662.

Krivácsy, Z., Kiss, G., Ceburnis, D., Jennings G., Maenhaut, W., Salma, I., Shooter, D., 2008. Study of water-soluble atmospheric humic matter in urban and marine environments. Atmos. Res. 87, 1-12.

Lavi, A., Lin, P., Bhaduri, B., Carmieli, R., Laskin, A., Rudich, Y., 2017. Characterization of light-absorbing oligomers from reactions of phenolic compounds and Fe(III). ACS Earth Space Chem. 1, 637-646.

Li, Y. J., Huang, D. D., Cheung, H. Y., Lee, A. K. Y., Chan, C. K., 2014. Aqueous-phase photochemical oxidation and direct photolysis of vanillin – a model compound of methoxy phenols from biomass burning. Atmos. Chem. Phys. 14, 2871-2885.

McNeill, V. F., Woo, J. L., Kim, D. D., Schwier, A. N., Wannell, N. J., Sumner, A. J., Barakat, J. M., 2012. Aqueous-phase secondary organic aerosol and organosulfate formation in atmospheric aerosols: A modeling study. Environ. Sci. Technol. 46, 8075-8081.

Mekic, M., Loisel, G., Zhou, W., Jiang, B., Vione, D., Gligorovski, S., 2018. Ionic strength effects on the reactive uptake of ozone on aqueous pyruvic acid: Implications for air-sea ozone deposition. Environ. Sci. Technol. 52, 12306–12315.

Net, S., Nieto-Gligorovski, L., Gligorovski, S., Temime-Rousell1, B., Barbati, S., Lazarou, Y. G., Wortham, H., 2009. Heterogeneous light induced ozone processing on the organic coatings in the atmosphere. Atmos. Environ. 43, 1683-1692.

Paulson, S. E., Liu, D. L., Orzechowska, G. E., 2006. Photolysis of heptanal. J. Org. Chem. 71, 6403-6408.

Popovicheva, O. B., Persiantseva, N. M., Tishkova, V., Shonija, N. K., Zubareva, N. A., 2008. Quantification of water uptake by soot particles. Environ. Res. Lett. 3, article 025009.

Reinhardt, A., Emmenegger, C., Gerrits, B., Panse, C., Dommen, J., Baltensperger, U., Zenobi, R., Kalberer, M., 2007. Ultrahigh mass resolution and accurate mass measurements as a tool to characterize oligomers in secondary organic aerosols. Anal. Chem. 79, 4074-4082.

Rosenfeld, D., Lohmann, U., Raga, G. B., O'Dowd, C. D., Kulmala, M., Fuzzi, S., Reissell, A., Andreae, M. O., 2008. Flood or drought: How do aerosols affect precipitation? Science 321, 1309-1313.

Ruehl, C. R., Davies, J. F., Wilson, K. R., 2016. An interfacial mechanism for cloud droplet formation on organic aerosols. Science 351, 1447-1450.

Schurman, M. I., Boris, A., Desyaterik, Y., Collett, Jr., J. L., 2018. Aqueous secondary organic aerosol formation in ambient cloud water photo-oxidations. Aerosol Air Qual. Res. 18, 15-25.

Schwartz, S. E., Andreae, M. O., 1996. Uncertainty in climate change caused by aerosols. Science 272, 1121-1122.

Shi, Q., Pan, N., Long, H., Cui, D., Guo, X., Long, Y., Chung, K. H., Zhao, S., Xu, C., Hsu C. S., 2012. Characterization of middle-temperature gasification coal tar. Part 3: Molecular composition of acidic compounds, Energy & Fuels 27, 108-117.

Simoneit, B. R. T., 2002. Biomass burning - a review of organic tracers for smoke from incomplete combustion. Appl. Geochem. 17, 129-162.

Srivastava, D., Tomaz, S., Favez, O., Lanzafame, G. M., Golly, B., Besombes, J.-L., Alleman, L. Y., Jaffrezo, J.-L., Jacob, V., Perraudin, E., Villenave, E., Albinet, A., 2018. Speciation of organic fraction does matter for source apportionment. Part 1: A one-year campaign in Grenoble (France). Sci. Total Environ. 624, 1598–1611.

Sun, Y., Zhang, Q., Anastasio, C., Sun, J., 2010. Insights into secondary organic aerosol formed via aqueous-phase reactions of phenolic compounds based on high resolution mass spectrometry, Atmos. Chem. Phys. 10, 4809-4822.

Tang, R.Z., Li, H.X., Liu, Y.C., Zhang, P., Cao, X.Y., Wang, W.F., 2012. Laser flash photolysis study on electron transfer oxidation reaction of tryptophan or tyrosine with triplet state vitamin K-3. Acta Phys. Chem. Sinica 28, 213-216.

Valero, N., Gomez, L., Pantoja, M., Ramirez, R., 2014. Production of humic substances through coal-solubilizing bacteria. Braz. J. Microbiol. 45, 911-918.

Wang, X., Hayeck, N., Brüggemann, M., Yao, L., Chen, H., Zhang, C., Emmelin, C., Chen, J., George, C., Wang., L., 2017. Chemical characteristics of organic aerosols in Shanghai: A study by ultrahigh-performance liquid chromatography coupled with Orbitrap mass spectrometry. J. Geophys. Res. Atmos., 122, 11703-11722.

Windsor, M. W., 2003. Flash photolysis and triplet states and free radicals in solution. Photochem. Photobiol. Sci. 2, 455-458.